

# RSC Advances



This is an *Accepted Manuscript*, which has been through the Royal Society of Chemistry peer review process and has been accepted for publication.

*Accepted Manuscripts* are published online shortly after acceptance, before technical editing, formatting and proof reading. Using this free service, authors can make their results available to the community, in citable form, before we publish the edited article. This *Accepted Manuscript* will be replaced by the edited, formatted and paginated article as soon as this is available.

You can find more information about *Accepted Manuscripts* in the [Information for Authors](#).

Please note that technical editing may introduce minor changes to the text and/or graphics, which may alter content. The journal's standard [Terms & Conditions](#) and the [Ethical guidelines](#) still apply. In no event shall the Royal Society of Chemistry be held responsible for any errors or omissions in this *Accepted Manuscript* or any consequences arising from the use of any information it contains.

# Integrated microfluidic device for the spherical hydrogel pH sensor fabrication

Yawei Sun,<sup>a</sup> Yaopeng Zhang,<sup>\*a</sup> Jingjing Liu<sup>\*b</sup> and Fuqiang Nie<sup>\*b</sup>

a. State Key Laboratory for Modification of Chemical Fibers and Polymer Materials, College of Materials Science and Engineering, Donghua University, Shanghai, 201620, China. E-mail: [zyp@dhu.edu.cn](mailto:zyp@dhu.edu.cn);

b. Suzhou Institute of Nano-Tech and Nano-Bionics, Chinese Academy of Sciences, Division of Nanobionic Research, Suzhou, 215123, China. E-mail: [jjliu2015@sinano.ac.cn](mailto:jjliu2015@sinano.ac.cn); [fqnie2012@sinano.ac.cn](mailto:fqnie2012@sinano.ac.cn).

In this work, hydrogel photonic crystal beads with inverse opal structure are generated on a well-controlled microfluidic chip device. An online droplet drying method and templating technique are integrated into the producing process. This process results in the silica nanoparticles in the droplets self-assembled into spherical photonic crystals with narrow stop bands and identical structural colours, which is the ideal template for fabricating inverse opal hydrogel beads. The effects of acrylic acid (AA) concentration, water dosage and buffer pH on the equilibrium swelling of inverse opal hydrogel are discussed. In the concentration of AA (3%) and water (31%), the inverse opal hydrogel beads show wide sensing range and rapid response (less than 30s) to pH variation. Overall, the inverse opal hydrogels as pH sensors show homogeneous structural colour changes due to the spherical 3D structure. The present characterization of quite mechanically robust and good reproducibility for the spherical pH sensor may have promise application in advanced optical devices.

## Introduction

Owing to the angle-independent structural colours, photonic crystal microparticles with three-dimensional ordered structure have showed a great applications in label-free multiplex detection<sup>1, 2</sup> and in the constructing of

angle-independent optical devices.<sup>3</sup> Inverse opal hydrogel with a typically 3D periodically ordered macropores array that is formed from functionalized hydrogels is a good candidate for chemical and biological sensors.<sup>4-8</sup> In order to fabricate inverse opal hydrogel, photonic crystal beads templates are usually employed.<sup>2</sup> Among many technology used for droplet fabrication,<sup>9-12</sup> microfluidic technology provides fine control over size and structure, which has been recently arisen as a simple method to fast fabricate PhC (Photonic Crystal) materials, especially to obtain droplets for the generation of PCBs,<sup>13-16</sup> which could be typically created by evaporating solvent droplets that contain colloidal nanoparticles.<sup>17-20</sup>

Since ordered macroporous polymer hydrogels exhibit large reversible volume changes in response to external stimuli, such as pH, ions, temperature or electric field,<sup>21-23</sup> which leading to a readable change in optical diffraction accompanied by a visually perceptible colour change, it would be the best material to fabricate pH sensor. Some studies also used polymer hydrogel and photonic crystal to fabricate various types of sensors<sup>24-26</sup> and bionic structural colour materials<sup>27</sup> due to the regulatory photonic band gap. Lee and Braun<sup>21</sup> first synthesized thin ( $\sim 23 \mu\text{m}$ ) inverse opal hydrogels film through colloidal crystal templating method, which make a breakthrough on the pH sensor. However, since the colour change on the film varied when observed from different angle, this angle dependence limits the application of pH sensor. Compared to films, the inverse opal hydrogel beads have advantages of identical structural colour and stop-band gaps derived from PCBs. In addition, the uniform macropores through the inverse opal hydrogel provide higher specific surface area, faster ion diffusion and more interaction sites, resulting in more sensitive to external stimulus. Thus, there is still a challenge to achieve a high pH sensitive and fast response of inverse opal hydrogel which could be identified by angle-independent colour.

In this study, we report a simple microfluidic chip equipped with on line collecting device to fabricate photonic crystal beads. Integrated digital control of fluids, on line direct droplet solidification and collection, the chip show advantages of fast generation and controllable operation. Monodisperse droplet templates and PCBs can be produced efficiently and reproducibly. Furthermore, by using  $\text{SiO}_2$  PCBs as templates, we synthesized inverse opal hydrogel pH

sensors based on photo-polymerization of 2-hydroxyethyl methacrylate and acrylic acid (HEMA/AA). Several different compositions of AA and water in hydrogel precursors are chosen to examine the pH sensitivities, and the high sensitive inverse opal hydrogels exhibit tunable colour changes which almost covering the entire wavelength of visible light. In addition, materials with these inverse opal hydrogel pH sensors show optical diffraction shift along with volume variation that could be useful for drug-delivery or other potential optical devices.

## Experimental

### Microfluidic Device

The size-controlled droplet templates were generated by using a cuboids glass microfluidic chip (26 mm\*76 mm\*2 mm, WenHao Chip Technology CO., LTD) with a cross channel (300  $\mu\text{m}$  in depth and 200  $\mu\text{m}$  in width) (Fig. 1). Two lateral channels were injected with oil phase while the main channel with water phase by PTFE soft tubing (0.5 mm\*1.58 mm) attached to syringes that were driven by digital syringe pumps (JSRC, RSP02-B). The PEEK joints (1.6 mm\*6 mm) were fixed on the inlets of microfluidic chip by a transparent acrylic structural adhesive.

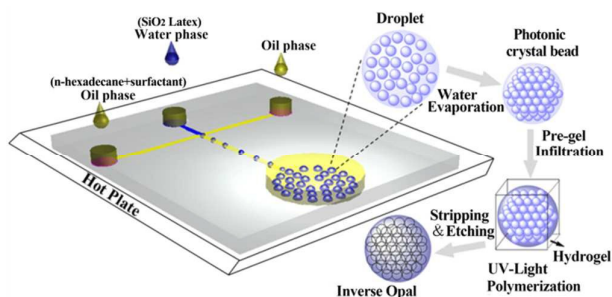


**Fig. 1** The schematic diagram for fabricating photonic crystal beads and the inverse opal hydrogel beads.

### Preparation of droplet templates and PCBs

The 15% w/v SiO<sub>2</sub> latex (particle diameter: 240 nm, polydispersity  $\leq 2.5\%$ , Nanjing Dongjian Biological Technology CO., LTD) was used as dispersed phase, while the continuous phase was n-hexadecane (Aladdin) containing 1% wt surfactant (Hypermer 2296, Croda), which stabilized the W/O interface of the droplets. The dispersed phase was ultra-sonicated (Jiekang, PS-20A) for 20

min before use. The channels were treated with a hydrophobic reagent (Trimethoxy(octadecyl)silane, Aladdin) before the oil phase was pumped into the chip to discharge air bubbles. After that, the oil phase stopped until the dispersed phase formed a continuous flow. The system reached steady state in less than 5 min. The droplets generated at the cross point, flowed through the main channel and finally hexagonally gathered at the rounded outlet. The droplets in different size were obtained by changing the injection rates. With a heating plate (ZNCL-B), the continuous droplets were online dried at 80 °C for 3 h. As the droplets in the outlet was heated constantly by the heating plate, the water in the droplets started to evaporate as soon as the droplets entered the outlet, as shown in Fig. 1. The silica nano-particles in the droplets gradually self-assembled into ordered lattices and the structural colours appear when the water evaporates. Eventually, PCBs were achieved when the water was evaporated completely. Then, to improve their mechanical property, the PCBs were sintered in a muffle furnace (Jing Hong, SXL-1208) at 800 °C for 3 h.

#### **Preparation of spherical inverse opal hydrogel pH sensor**

The pH sensitive hydrogel precursors with 1% wt AA, 19.2% wt H<sub>2</sub>O, were composed of 2.5 g 2-hydroxyethyl methacrylate (HEMA,TCL), 25 mg Ethylene glycol dimethacrylate (EGDM, Aladdin), 75 mg Irgacure-651 (TCL), 35 mg Acrylic acid (AA, Enox) and 0.625 g DI-water. By changing AA and DI-water content respectively, four other kind of precursor were obtained: 3% wt AA, 18.8% wt H<sub>2</sub>O (100 mg, 625 mg); 5% wt AA, 18.2% wt H<sub>2</sub>O (170 mg, 625 mg); 3% wt AA, 31% wt H<sub>2</sub>O (120 mg, 1.25 g); 3% wt AA, 40% wt H<sub>2</sub>O (170 mg, 1.875 g). All monomers were mixed in a vial, and ultra-sonicated for 10 min before use. A typical procedure for the preparation of hydrogel sensor is illustrated in Fig. 1. With air pressure and capillary action facilitated, the pH sensitive hydrogel precursor infiltrated into the interstices between the silica nanoparticles of the PCBs templates which turned into transparent after completely penetration.

Subsequently, the hydrogel precursor was thoroughly polymerized through the PCBs using a portable UV-lamp (Yuezhong) at 365 nm for 2 h with 15 mm distance between lamp and the samples. After immersed in the DI-water for 30 min, the hybrid PCBs in the hydrogel film were split readily, it could be

explained that the hydrogel outside the PCBs exhibited a certain degree of swelling, while the hydrogel in the interstices of the PCBs did not swell because of the restriction of the close-packed template. After etching SiO<sub>2</sub> colloidal templates with 10% hydrofluoric acid (caution the danger of the HF) for 24 h, the hydrogel beads with inverse opal structure were obtained eventually. The hydrogel beads were soaked in DI-water for further use. Using a pH meter (PHS-3E, INESA), the phosphate buffer solutions were prepared by mixing KH<sub>2</sub>PO<sub>4</sub> (0.1 M, Enox) with different volumes of HCl (0.1 M, Enox) and NaOH (0.1 M, Enox).

### **Characterization**

The formation of droplets was monitored with a CCD (HDCE-X3) attached to a stereo microscope (JSZ5, JiangNan). Photographs of droplets, PCBs and the colour change of the inverse opal hydrogel beads were captured by a digital camera (D3100, Nikon) under illumination of white LED lamp and an optical microscope (OLYMPUS BX51) equipped with a CCD camera (Media Cybernetics Evolution MP 5.0). Reflection spectra of the PCBs and the inverse opal hydrogel beads were recorded using a microscope equipped with a fiber optic spectrometer (Ocean Optics, QE 65000). After froze in -80°C refrigerator, the inverse opal hydrogel beads were dried in a desktop vacuum freeze dryer (Free Zone 2.5 Liter, Labconco). After all the samples were coated with gold in a small ion sputtering apparatus (Beijing HTC Technology, JS-1600), the microstructures of the PCBs and the derived inverse opal hydrogel beads were characterized using a field emission environmental scanning electron microscopy (Quanta FEG 250, FEI).

## **Results and discussion**

### **Preparation of size-controlled droplets and PCBs templates**

Controllable uniform emulsion droplets on the micrometre scale are produced using a microfluidic chip with a cross channel (Fig. 1). The W/O droplets are formed under the shearing force of the continuous phase from the lateral channels. Monodispersed emulsion droplets ranging from tens to hundreds of micrometres in average diameter are produced by simply changing the velocity

of the water ( $V_w$ ) and the oil phase ( $V_o$ ). Two sets of experiments are performed in the same microfluidic chip. Fig. 2a shows that the velocity of the oil phase fixe at  $0.1 \mu\text{l/s}$  while the water phase increase from  $0.03 \mu\text{l/s}$  to  $0.35 \mu\text{l/s}$ . It is found that  $D_0$  exhibits linear growth from  $370 \mu\text{m}$  to  $530 \mu\text{m}$ . In comparison, when the velocity of the oil phase increase from  $0.1 \mu\text{l/s}$  to  $0.45 \mu\text{l/s}$  under the condition of  $V_o = 0.1 \mu\text{l/s}$ ,  $D_0$  exhibits an linear decay from  $396 \mu\text{m}$  to  $296 \mu\text{m}$ , as shown in Fig. 2b. Overall, the droplets diameter decays as the velocity of the oil phase increasing. This relationship between diameter ( $D_0$ ) and velocity ( $V_o$ ) is similar with the describes of other studies.<sup>28</sup>

Similar with classic T-junction microfluidic chip,<sup>18</sup> the cross channel of the chip is designed to generate droplets efficiently in this study. As calculated in Fig. 2d, the size distribution of the droplets gives a polydispersity ( $\sigma/d$ ,  $\sigma$  is the standard deviation of the droplet diameter,  $d$  is the average diameter of 200 droplets) of less than 0.3%. The low polydispersity of the droplets should be attributed to the stable generation process. High-quality droplets can be fast generated for further application. Compared to capillary microfluidic device,<sup>29</sup> this microfluidic device show more convenience and stability for the fabrication of  $\text{SiO}_2$  PCBs because that all the procedures are integrated into the microfluidic chip.

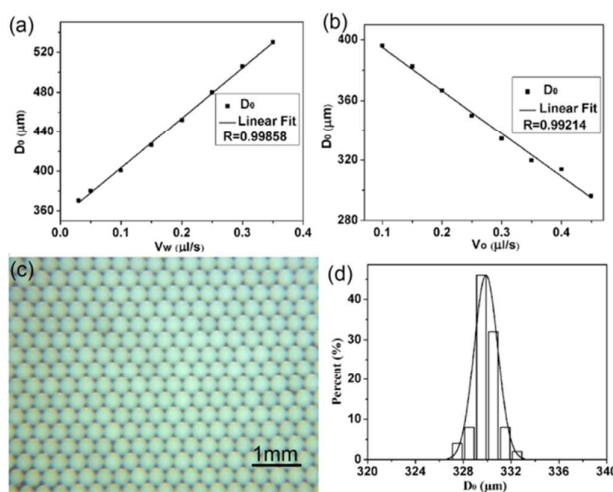


**Fig. 2** (a) Relationships between the droplets sizes  $D_0$  and the velocity of water phase ( $V_o=0.1 \mu\text{l/s}$ ) and (b) the velocity of oil phase (with  $V_w=0.1 \mu\text{l/s}$ ); each point is an average diameter of 100 droplets; (c) The monodispersed aqueous droplets of 330 nm in diameter containing colloidal  $\text{SiO}_2$  particles, when the velocities of water and oil phase are set at  $0.1 \mu\text{l/s}$  and  $0.3 \mu\text{l/s}$  respectively; (d) Size distribution of 200 droplets.

In this experiment, the droplets are generated, collected and dried directly on the chip. Generally, the generated droplets are transported to the oven for drying. However, during the transportation, the droplets are readily to break and converge into larger droplets. With our microfluidic chip device, this variation could be eliminated. As long as  $\text{SiO}_2$  particles are stable in liquid and their size distribution is sufficiently narrow, they could crystallize into a face centred cubic (FCC) lattice<sup>30</sup> by increasing their volume fraction through concentration process like controlled evaporation. When the oil in the outlet being constantly heated, the water in the droplets start to evaporate, the silica nanoparticles gradually self-assemble into ordered lattices and appear iridescent colour. Eventually, the beads show a characteristic opaline colour in water (Fig. 3a) and in air (Fig. 3b), which is a clear evidence of the formation of photonic crystal. The consolidation time and the size of the PCBs depend on the drying temperature, the concentration of the silica nanoparticles in latex, and the diameter of the droplets.

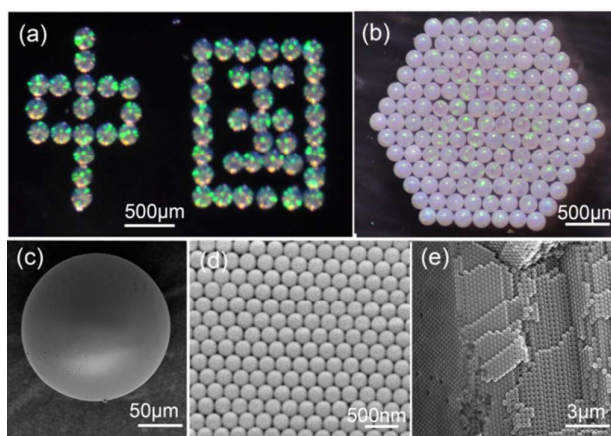


**Fig. 3** Images of PCBs: (a) in water and (b) in air; SEM images of PCBs: (c) low-magnification image, (d) high-magnification images of the surface structure and (e) the inner structure.

The silica nanoparticles of the PCBs mainly formed a close-packed FCC structure in the sphere. It can be observed that the PCBs have excellent spherical structures and smooth surfaces (Fig. 3c). The enlarged SEM image shows that the nanoparticles on the PCBs surface arrange in predominantly hexagonal symmetry (Fig. 3d) which extend to the inside of the whole beads (Fig. 3e). This structure imparts photonic band-gaps (PBGs) and characteristic reflection peaks to PCBs. Characteristic reflection peaks are a remarkable

property of the photonic crystals. Under normal incidence, the peak value can be estimated by Bragg's Law<sup>31</sup>:

$$\lambda = 1.633D_{particle}n_{eff} \quad (1)$$

where  $\lambda$  is the peak wavelength of the reflected light,  $D_{particle}$  is the centre-to-centre distance between two neighbouring silica nanoparticles, and  $n_{eff}$  is the average refractive index of the PCBs and the medium (such as water). In addition, the PCBs exhibit uniform sphericity with narrow size distribution, they show identical photonic responses which are independent of the rotation of the axes.<sup>3</sup> That is, the PCBs exhibit identical structural colours from all observing perspectives. With these ideal characteristics, the PCBs are appropriate as templates for the fabrication of hydrogel sensors.

### **Fabrication of inverse opal hydrogel Beads**

Preparation of inverse opal hydrogel beads require multiple experimental steps which strongly affect the sensitivity and mechanical properties of the final beads. To achieve fast response pH sensor, it's crucial to optimize the photopolymerization conditions such as exposure time, intensity, and wavelength of UV-lamp. Because the crosslinking density of hydrogel and the size of holes between voids are the most important decisive factors for the colour change. A direct exposure of UV-365 nm for 2 h with a 15 mm distance result in a nearly homogeneously polymerized structure.<sup>32</sup> After etching, the hydrogel beads achieve highly iridescent colour in water (Fig. 4a) and the original FCC structure of SiO<sub>2</sub> colloidal crystal are well transformed into an inverse opal structure which primarily consists of void spaces and interconnected holes (Fig. 4c, d). Compared to the inverse opal hydrogel films,<sup>21</sup> the spherical structure of the inverse opal hydrogel beads gives rise to swell or shrink at all directions which imparts it with angle-independence property like PCBs templates. Besides, compared to the diameter of SiO<sub>2</sub> particle in PCBs templates (Fig. 3d, 240 nm), the size of the voids in the inverse opal have a little shrinkage (Fig. 4d, 230 nm) which may be caused by the shrinkage of hydrogel in the process of freeze drying.

Besides, there are some disorder occurred in the inverse opal hydrogel beads and the disordered parts could give the hydrogel beads a variegated colour from its original homogeneous structural colour (Fig. 4a, Fig. S1, Supporting Information). As shown in Fig. 4b, the defects in the inverse opal hydrogel that may derive from drying cracks and crystal defects of the colloidal template,<sup>26</sup> are filled with hydrogel and tend

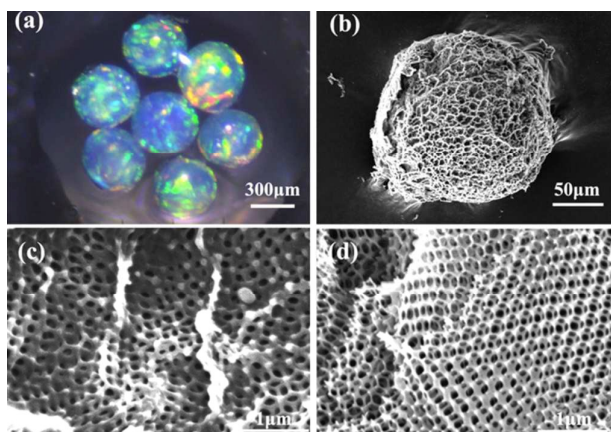


**Fig. 4** (a) Optical microscope image of the 1% AA, 19% H<sub>2</sub>O inverse opal hydrogel; SEM images of inverse opal hydrogel beads: (b) low-magnification image; (c) high-magnification image of the surface; (d) the inner section structure.

to swell more drastically than the rest of the porous hydrogel network which may cause the hydrogel to increasing disorder during swelling. Besides, the higher swelling in the defect sites may create local stress points that may buckle the surrounding structures, resulting in a large scatter in the normalized full width at half maximum (FWHM) values and inhomogeneous structural colour in some hydrogel beads. Some defects may be contributed by template etching process and needle prick operated by a needle. Despite that the defects may affect the pH response measurement in a way, the main colour change is clearly readable for naked-eye detection.

#### **pH sensitivity of inverse opal hydrogel Beads**

As previous said, the inverse opal hydrogel beads primarily consist of void spaces and interconnected hydrogel network. When the beads are put into pH buffer, the diffusion of ion take place both through the void space and the hydrogel network. The swelling and deswelling abilities of the hydrogel beads rely on the crosslinking density of hydrogel and the size of holes between voids. The photographs and reflection spectra of the PCBs template and five kind of hydrogel beads in pH=6 buffer solution are plotted in Fig. 5. The brilliant colour of the hydrogel beads with different concentration of AA and H<sub>2</sub>O are derived by their periodic ordered porous structure, which corresponding to their peak position in the reflection spectra.

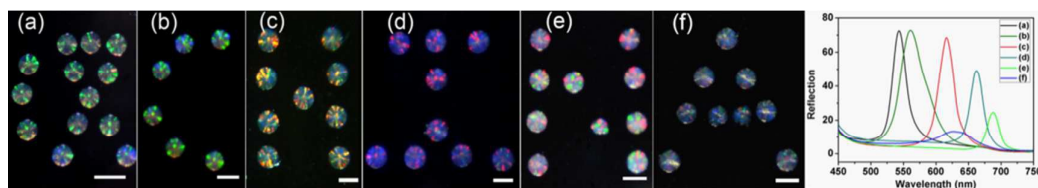


**Fig. 5** Optical microscope images depicting the colour change and reflection spectra in pH=6 buffer: (a) PCBs array; the inverse opal hydrogel beads: (b) 1% AA, 19.2% H<sub>2</sub>O; (c) 3% AA, 18.8% H<sub>2</sub>O; (d) 5% AA, 18.2% H<sub>2</sub>O; (e) 3% AA, 31% H<sub>2</sub>O; (f) 3% AA, 40% H<sub>2</sub>O; the scale bar is 600  $\mu$ m.

According to the Bragg's Law (Equation (1)), the diameter of the silica nanoparticle is about 240 nm in the PCBs templates (Fig. 5a), and the average refractive index ( $n_{\text{eff}}$ ) of the PCBs close-packed structure is approximately 1.35 ( $n_{\text{eff}}^2 = n_{\text{silica}}^2 \eta + n_{\text{buffer}}^2 (1 - \eta)$ , where  $n_{\text{silica}} = 1.45$ ,  $n_{\text{buffer}} = 0.98$ ,  $\eta = 0.74$ ), the calculated reflection peak is 527 nm, which is close to the detected peak position value of 541 nm. With regard to the inverse opal hydrogel beads, the  $n_{\text{eff}}$  is about 1.14 ( $n_{\text{eff}}^2 = n_{\text{buffer}}^2 \eta + n_{\text{hydrogel}}^2 (1 - \eta)$ ,  $n_{\text{buffer}} = 0.98$ ,  $n_{\text{hydrogel}} = 1.51$ ), the peak position is mainly attributed to the size of holes ( $D_{\text{particle}}$ ). For instance, in the buffer solution of pH 6, the detected peak position of the 1% AA, 19.2% H<sub>2</sub>O hydrogel beads is 560 nm. The diameter of this hydrogel beads is about 450  $\mu$ m (Fig. 5b) which is much higher than the diameter of the PCBs template (260  $\mu$ m, Fig. 5a), hence, the void size is far above the SiO<sub>2</sub> particle size. The consistency of the peak position between estimated values and the experimental measurements show that the products are qualified in optical properties. Furthermore, the hydrogel beads exhibit well-ordered macroporous structure not only can be proved by Fig. 4d, but also can be detected by the value of FWHM as narrow as 40 nm at the reflection spectra.

As the acrylic acid (AA) concentration increasing in hydrogel beads (Fig. 5b, c, d), they show higher swelling with diameter 450 $\mu$ m, 525 $\mu$ m, 560 $\mu$ m and their detected peak position red shift, which are 560 nm, 616 nm and 668 nm respectively. Besides, as the water dosage increasing (Fig. 5c, e, f), the optical reflection peak should also red shift as expected because their crosslinking density decrease. However, the detected peak position of (c), (e) and (f) are 616 nm, 687 nm and 626 nm respectively. The abnormality peak position of (f) may be caused by adding too much water content in hydrogel precursor which made the concentration of the crosslinking agent (EGDM) too low to form a perfect hydrogel network. Compare to other samples, the disorder structures through the beads made this hydrogel bead exhibit poor swelling behaviour,

little red shift, wide FWHM, poor iridescent colour and low reflection intensity. In addition, as shown in the reflection spectra in Fig. 5, the decreased of diffraction peak intensity from (a) to (f) could be explained by a number of causes such as continuously emerge of disorder and partial pore close during hydrogel expansion.

To further evaluate the effect of the AA concentration, water dosage and buffer pH on the equilibrium swelling of inverse opal hydrogel, four kinds of hydrogel beads are tested under the stimulation of buffer solution with different pH value. Since the same diameter sacrificial SiO<sub>2</sub> particles are used for all cases, the crosslinking density of the hydrogel is the only reason for the apparent  $\lambda_{\max}$  difference at the same pH buffer (Fig. 6a). The degree of pH sensitivity varies with the different composition of hydrogel. As shown in Fig. 6a, the hydrogel beads become more sensitive as the AA concentration increasing. Similarly, with the same composition of AA (3%), the best sensitive could be depended on the water dosage of the hydrogel, which show larger  $\lambda_{\max}$  variation of high percentage H<sub>2</sub>O (31%) in the hydrogel beads than lower percentage of H<sub>2</sub>O (18%).

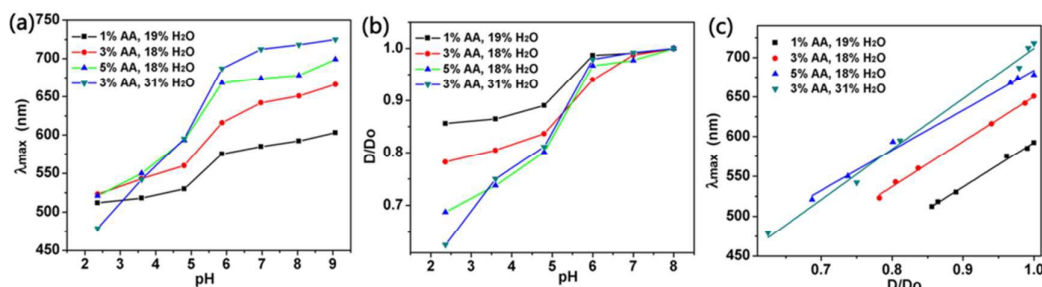


**Fig. 6** (a) Dependence of the diffraction peak position ( $\lambda_{\max}$ ) of four different hydrogel beads on pH increasing; (b) Dependence of the swelling degree ( $D/D_0$ ) of four different hydrogel beads on pH increasing; (c) Plot of the relationship between the diffraction peak position ( $\lambda_{\max}$ ) and swelling degree ( $D/D_0$ ).

As the pH value of buffer increasing, the swelling degree ( $D/D_0$ ) of the hydrogel beads significantly increase due to the ionization equilibrium between the carboxyl group in acrylic acid and the ion in buffer solution which result in perceptible colour change and reversible swelling (Fig. 6b). As shown in Fig. 6c, a larger unit lattice size (distance between pores) within the inverse opal structure resulted in a more red-shifted  $\lambda_{\max}$  corresponding to the Bragg's Law (Equation (1)). When hydrogel beads swell, the buffer solution fill pores, the hydrogel network keep stay on the ordered porous lattice. Diffraction response kinetics could be modelled as a hindered diffusion-limited process,<sup>33</sup> where H<sup>+</sup> and OH<sup>-</sup> ions, diffusing from the bulk solution

into the gel phase as a result of a concentration gradient, are eliminated when they come into contact with immobilized deprotonated/protonated acid moieties on the network.

The 0.1 M potassium phosphate ( $\text{KH}_2\text{PO}_4$ ) buffer mix with 0.1 M HCl and/or 0.1 M NaOH are used since the buffering pH range exactly covers the most sensitive pH range of HEMA/AA hydrogel system (around pH 5-6) as illustrated in Fig. 6a. Since most of AA units are deprotonated by a pH of 8, as pH increase over 7,  $\lambda_{\text{max}}$  red shift slightly, the corresponding colour change is not recognizable because red colour is located at the long wavelength edge of the visible spectrum. By applying pH buffer below 5,  $\lambda_{\text{max}}$  further blue-shift and the hydrogel exhibit explicit colour change. The beads have fast response less than 30 s when pH varies from 5 to 6 (Fig. S2, Supporting Information). The rapid pH response may be mainly attributed to two factors: the small volume of the hydrogel beads (micrometre size); the well-ordered porous structure in which the molecules or ions could diffuse rapidly. Overall, as shown in Fig. 6, among the hydrogel beads, the mixed ratio with 3% AA, 31%  $\text{H}_2\text{O}$  of hydrogel precursors has the relative high pH sensitivity ( $D/D_0$ ) and wide pH response region (pH 1-9).

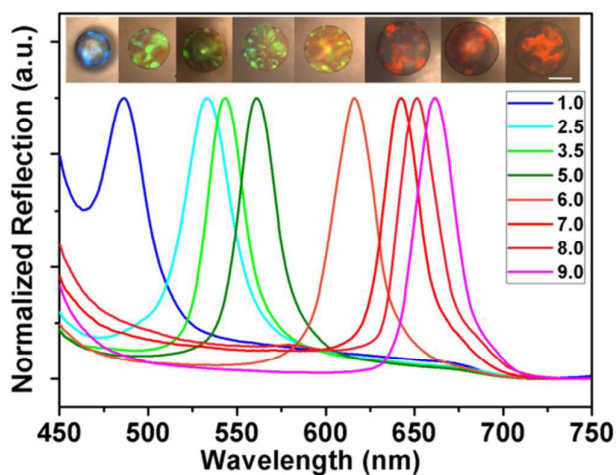


**Fig. 7** Microscope images of colour change and a series of reflection spectra of d (3% AA, 18.8%  $\text{H}_2\text{O}$ ) inverse opal hydrogel beads are obtained during pH increased from 1.0 to 9.0; from left to right, each image corresponds to a spectrum; the scale bar is 200  $\mu\text{m}$ .

Furthermore, during pH increases, the perceptible structural colour changes could be detected by optical spectra instruments (Fig. 7), the colour of hydrogel beads with 3% AA, 18.8%  $\text{H}_2\text{O}$  concentration varies from initial blue to green then yellow

and orange, finally red.. The brilliant colours cover almost the whole wavelength of visible lights, which is perfect for naked-eye detection in further development.

Now that the hydrogel sensor selectively responds to the pH variation, there may exist complex ion equilibria in the mixed buffer system which could affect Donnan equilibrium exerted by proton. When the pH value of buffer solution is low, the hydrogel chains curl up because the high concentration of  $H^+$  restrain the dissociation of the carboxyl group (-COOH) in the hydrogel. As pH increasing, -COOH begin to dissociate, the hydrogen bonds between chains are destroyed while the crosslinking points are decayed, which give rise to the increase of electrostatic repulsion, the bonds stretching, eventually lead to expanding of the hydrogel network. Besides, the derived  $-COO^-$  also make the hydrogel expand by its hydrophilic property. The inverse opal hydrogel beads exhibit pH-dependent shifts in optical diffraction. The general shape of the peaks remains unchanged, suggesting that the overall layered microstructure of the template hydrogel could maintain during swelling. The hydrogel sensor demonstrate the good repeatability, fast responsive to pH value without visible degradation of iridescence or mechanical robustness even after it is completely dried or multiple pH tests (Fig. S3, Supporting Information).

## Conclusion

In this paper, we present a highly accessible method for producing a large sensitive range pH sensor. An online collection and drying is integrated into the microfluidic chip to fabricate PCBs by continuous droplets, which make the approaches efficiency and simplicity because the part of droplets transportation to the oven is omitted. Since the digital syringe pumps offer stable driving force, it can generate continuous droplets with low polydispersity.

A series of pH distinctive inverse opal hydrogel beads could be achieved by using different composition of hydrogel precursor. The optical diffraction shift may rely on the concentration of AA and water varied, which make difference in the swelling and deswelling of hydrogel, and the size of holes. When the concentration of AA and water is 3% and 31% respectively, the hydrogel shows best pH response and widest pH sensing range. These hydrogel pH sensors possess a series of desirable features including angle-independence, high sensitivity and quick response, which could be better applied in drug delivery, catalysis, and film separations in the future.

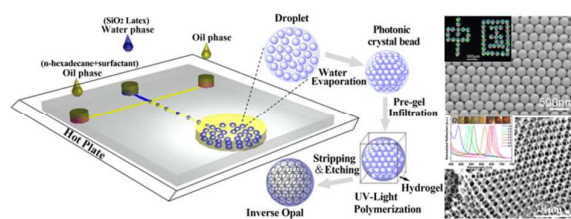
## Acknowledgements

This work is supported by the National Natural Science Foundation of China (21271182, 21274018), the Programme of Introducing Talents of Discipline to Universities (No.111-2-04), DHU Distinguished Young Professor Program (A201302) and the Fundamental Research Funds for the Central Universities (2232013A3-11).

## References

1. Y. Zhao, X. Zhao, J. Hu, M. Xu, W. Zhao, L. Sun, C. Zhu, H. Xu and Z. Gu, *Advanced Materials*, 2009, **21**, 569-572.
2. B. Ye, H. Ding, Y. Cheng, H. Gu, Y. Zhao, Z. Xie and Z. Gu, *Advanced Materials*, 2014, **26**, 3270-3274.
3. H. Gu, Y. Zhao, Y. Cheng, Z. Xie, F. Rong, J. Li, B. Wang, D. Fu and Z. Gu, *Small*, 2013, **9**, 2266-2271.
4. J. H. Holtz and S. A. Asher, *Nature*, 1997, **389**, 829-832.
5. N. Griffete, H. Frederich, A. Maitre, S. Ravaine, M. M. Chehimi and C. Mangeney, *Langmuir*, 2012, **28**, 1005-1012.
6. J. Shin, S. G. Han and W. Lee, *Sensors and Actuators B: Chemical*, 2012, **168**, 20-26.
7. T. Kanai, D. Lee, H. C. Shum, R. K. Shah and D. A. Weitz, *Advanced Materials*, 2010, **22**, 4998-5002.
8. M. J. Banuls, R. Puchades and A. Maquieira, *Analytica Chimica Acta*, 2013, **777**, 1-16.
9. J. H. Moon, G. R. Yi, S. M. Yang, D. J. Pine and S. Bin Park, *Advanced Materials*, 2004, **16**, 605-609.
10. G. R. Yi, T. Thorsen, V. N. Manoharan, M. J. Hwang, S. J. Jeon, D. J. Pine, S. R. Quake and S. M. Yang, *Advanced Materials*, 2003, **15**, 1300-1304.
11. H. Y. Li, H. Q. Wang, A. H. Chen, B. Meng and X. Y. Li, *Journal of Materials Chemistry*, 2005, **15**, 2551-2556.
12. Y. Masuda, T. Itoh and K. Koumoto, *Advanced Materials*, 2005, **17**, 841-845.
13. T. Liao, Z. Guo, J. Li, M. Liu and Y. Chen, *Lab on a Chip*, 2013, **13**, 706-713.
14. K. Xu, J. Xu, Y. Lu and G. Luo, *Crystal Growth & Design*, 2014, **14**, 401-405.
15. L. Shang, F. Shangguan, Y. Cheng, J. Lu, Z. Xie, Y. Zhao and Z. Gu, *Nanoscale*, 2013, **5**, 9553-9557.
16. Y. Zhao, H. Gu, Z. Xie, H. C. Shum, B. Wang and Z. Gu, *Journal of the American Chemical Society*, 2013, **135**, 54-57.
17. W. Liu, L. Shang, F. Zheng, J. Lu, J. Qian, Y. Zhao and Z. Gu, *Small*, 2014, **10**, 88-93.
18. K. Xu, J.-H. Xu, Y.-C. Lu and G.-S. Luo, *Crystal Growth & Design*, 2013, **13**, 926-935.
19. S. H. Kim, J. G. Park, T. M. Choi, V. N. Manoharan and D. A. Weitz, *Nature Communications*, 2014, **5**, 3068.
20. L. Yang, J. Wang, Y. Zhang, Y. Luo, D. Li and Q. Meng, *Langmuir*, 2012, **28**, 4160-4167.
21. Y.-J. Lee and Paul V. Braun, *Advanced Materials*, 2003, **15**, 563-566.
22. J. Madsen and S. P. Armes, *Soft Matter*, 2012, **8**, 592-605.
23. J. Wang, Y. Hu, R. Deng, R. Liang, W. Li, S. Liu and J. Zhu, *Langmuir*, 2013, **29**, 8825-8834.
24. Y. Zhao, X. Zhao and Z. Gu, *Advanced Functional Materials*, 2010, **20**, 2970-2988.

25. J. Shin, S. G. Han and W. Lee, *Analytica Chimica Acta*, 2012, **752**, 87-93.
26. Y.-J. Lee, S. A. Pruzinsky and P. V. Braun, *Langmuir*, 2004, **8**, 3096-3106.
27. Q. Yang, S. Zhu, W. Peng, C. Yin, W. Wang, J. Gu, W. Zhang, J. Ma, T. Deng, C. Feng and D. Zhang, *ACS Nano*, 2013, **7**, 4911-4918.
28. I.-L. Ngo, T.-D. Dang, C. Byon and S. W. Joo, *Biomicrofluidics*, 2015, **9**, 024107.
29. H. Gu, F. Rong, B. Tang, Y. Zhao, D. Fu and Z. Gu, *Langmuir*, 2013, **29**, 7576-7582.
30. H.-F. Zhang, S.-B. Liu and X.-K. Kong, *Applied Physics B: Lasers and Optics*, 2013, **4**, 553-563.
31. Z. Z. Gu, S. Kubo, W. P. Qian, Y. Einaga, D. A. Tryk, A. Fujishima and O. Sato, *Langmuir*, 2001, **17**, 6751-6753.
32. J. Shin, P. V. Braun and W. Lee, *Sensors and Actuators B: Chemical*, 2010, **150**, 183-190.
33. M. J. Skaug, L. Wang, Y. Ding and D. K. Schwartz, *ACS Nano*, 2015, **9**, 2148-2156.



A type of inverse opal hydrogel pH sensor with homogeneous structural colour were generated from an integrated microfluidic chip.